


High-order harmonic generation from stretched C_2H_2 molecules in intense laser fields

Jianke Li ^{1,2}, Zheng Shu,³ Shilin Hu,^{4,*} Chengrui Bi,³ Anping Huang,¹ Zhisong Xiao,¹ Xiao-jing Liu,^{1,2,†} and Jing Chen ^{3,5}

¹*School of Physics, Beihang University, Beijing 100191, China*

²*School of Physical Science and Technology, ShanghaiTech University, Shanghai 201210, China*

³*Institute of Applied Physics and Computational Mathematics, P. O. Box 8009, Beijing 100088, China*

⁴*Laboratory of Quantum Engineering and Quantum Metrology, School of Physics and Astronomy, Sun Yat-Sen University (Zhuhai Campus), Zhuhai 519082, China*

⁵*Shenzhen Key Laboratory of Ultraintense Laser and Advanced Material Technology, Center for Advanced Material Diagnostic Technology, and College of Engineering Physics, Shenzhen Technology University, Shenzhen 518118, China*



(Received 5 June 2021; revised 12 December 2021; accepted 25 January 2022; published 9 February 2022)

We investigate the high harmonic generation from stretched acetylene molecules subjected to intense laser fields employing time-dependent Hartree-Fock methods. It is found that as the C-C and C-H bonds are stretched, the harmonic efficiency increases significantly due to the increased ionization of inner valence σ orbitals in the monochromatic field, while the harmonic yield will be limited by the strong depletion of the ground-state population under a certain bond length. Moreover, the harmonic emission is affected by the nonadiabatic electron dynamics from the multiorbital coupling effects. In addition, by introducing a two-color field scheme for different C-H bond configurations with the fixed C-C bond, the aforementioned harmonic efficiency will be further enhanced due to laser-induced strong excitation from inner valence orbitals to initially unoccupied orbitals. The above results would be helpful for further understanding multiorbital dynamics in the harmonic generation from polyatomic molecules.

DOI: [10.1103/PhysRevA.105.023105](https://doi.org/10.1103/PhysRevA.105.023105)

I. INTRODUCTION

As the foundation of attosecond science [1], high-order harmonic generation (HHG) from atoms and molecules has become one of the hottest topics over the last three decades. HHG can not only be used to generate table-top extreme ultraviolet (XUV) light sources and attosecond pulses, but also provide the tools to probe the atomic and molecular structures and ultrafast dynamics [2–6]. HHG can be well understood in the classical three-step model, in which the bound electron tunnels through the barrier formed by the Coulomb potential and the laser field into the continuum, then obtains energy in laser-driven acceleration, and, finally, recombines radiatively [7]. For molecules, the close energy gap and the different symmetries among several molecular orbitals lead to multiple ionization channels depending on the angle of molecular alignment [8,9], which has a significant effect on the subsequent HHG [6,10–13], such as the occurrence of multichannel interference minimum.

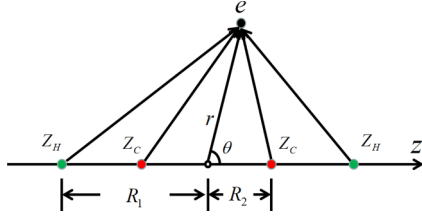
In addition to the complex electronic structure, the additional nuclear degrees of freedom for molecules also affects the ionization and harmonic generation. One example is the charge-resonance enhanced ionization (CREI) phenomenon, which indicates the appearance of high ionization rates at a critical internuclear distance R when molecules are exposed to intense laser pulses [14–16]. In the fixed-nuclei model,

the quantum interference between the two atomic centers will form a pronounced minimum in the harmonic spectra for suitable molecular alignment [17–19]. Afterwards, Lein further theoretically demonstrated that the harmonic intensity from the molecules with a lighter isotope is weaker with respect to that from molecules with a heavier isotope [20], which is interpreted by the nuclear vibrational autocorrelation function [21], and the above feature was subsequently confirmed by experimental observations [3]. The influence of nuclear motion on the HHG of small molecules has been extensively studied, mainly including the dynamic two-center interference effect [22], the isotope effect [23,24], the initial vibrational state effect [25,26], and the redshifts [27,28]. So far, most of the research mentioned above has mainly focused on one- and two-electron molecular systems or model molecules of reduced dimensionality. Some theoretical models based on the strong field approximation have been proposed to investigate the nuclear dynamics in HHG of multielectron molecules [29–32]. Nonetheless, accurate treatment of all electronic and nuclear dynamics in the study of molecular HHG remains challenging, especially for polyatomic molecules.

The purpose of our present study is to investigate the HHG of stretched polyatomic molecules using the time-dependent Hartree-Fock method (TDHF) [33–36]. We choose acetylene (C_2H_2) as the research object for the following two reasons: First, C_2H_2 is a simple and representative linear hydrocarbon molecule, which is essential in organic chemistry. For example, several works have focused on the impact of electronic structure on HHG of C_2H_2 molecules under midinfrared laser pulses [37,38]. Second, recent experiments have observed

*hushlin@mail.sysu.edu.cn

†liuxj@shanghaitech.edu.cn


 FIG. 1. Coordinates of the C_2H_2 molecule.

enhanced ionization in polyatomic molecules [39–44], and the above distinct feature is related to the increased ejection of inner-valence electrons in theoretical simulations [45–49]. Recently, Mulholland *et al.* showed that the excitation from the highest occupied molecular orbital (HOMO)-1 to the lowest unoccupied molecular orbital (LUMO)+1 plays a crucial role in the HHG of the C_2H_2 molecule by combining a vacuum ultraviolet laser pulse (the pump pulse) and midinfrared laser pulse (the probe pulse), and the electrons are described employing time-dependent density functional theory with the ions treated classically [50].

As stated above, a complete description of the roles of electron excitation and orbital coupling in the HHG of C_2H_2 molecules as a function of C-H and C-C bonding lengths, given in a detailed manner based on a quantitative analysis, is an intriguing problem, which is helpful for further understanding the multiorbital dynamics in molecular HHG. Moreover, the study of the enhanced harmonic efficiency of C_2H_2 molecules due to excitation from inner-valence orbitals to unoccupied orbitals induced by the auxiliary XUV field is required. In this work, we employ the TDHF approach to study the impact of orbital mixing, electronic excitation, and nonadiabatic effects on the HHG of C_2H_2 molecules with different bonding lengths exposed to monochromatic and two-color laser fields. It should be noted here that the nuclei are frozen in our calculations, and the reason is that taking accounting of nuclear motion will not only increase the numerical effort considerably, but also complicate the analysis of the questions considered, which is beyond the scope of the current work.

The present paper is organized as follows. In Sec. II, we present the TDHF theory to study HHG from stretched C_2H_2 molecules in intense linearly polarized laser fields. Section III contains the results and discussion. In Sec. III A, we show the HHG spectrum for C_2H_2 molecules with different C-H and C-C bonding lengths in the monochromatic fields and the contribution of different orbitals to HHG spectra. In Sec. III B, we introduce a two-color field scheme to investigate the effect of excitation from inner-valence orbitals to unoccupied orbitals induced by the auxiliary XUV field on the HHG spectra. Finally, the conclusions are given in Sec. IV. Atomic units (a.u.) are used, unless indicated otherwise.

II. THEORETICAL APPROACHES

Figure 1 shows the coordinates of the C_2H_2 molecules based on one-center expansion [34]. The C-C and C-H bond distances are defined as $R_{CC} = 2|\mathbf{R}_2|$ and $R_{CH} = |\mathbf{R}_1| - |\mathbf{R}_2|$, respectively. The equilibrium internuclear distances are $R_{CC} = 2.27$ a.u. and $R_{CH} = 2$ a.u. Two sets of calculations

are performed in our work: one is that the R_{CH} is changed with R_{CC} fixed at the equilibrium bond length, and another one indicates that both R_{CC} and R_{CH} are varied. The TDHF equation for C_2H_2 molecules subjected to laser pulses within the dipole approximation is written as [35,36,47]

$$i\frac{\partial}{\partial t}\Psi_i(\mathbf{r}, t) = [H_0(\mathbf{r}) + 2J(\mathbf{r}, t) - K(\mathbf{r}, t) + \mathbf{r} \cdot \mathbf{E}(t)]\Psi_i(\mathbf{r}, t), \quad (1)$$

where

$$H_0(\mathbf{r}) = -\frac{1}{2r^2}\frac{\partial}{\partial r}r^2\frac{\partial}{\partial r} - \frac{1}{2r^2}\left[\frac{\partial}{\partial\xi}(1-\xi^2)\frac{\partial}{\partial\xi} - \frac{m^2}{1-\xi^2}\right] - \frac{Z_H}{|\mathbf{r} + \mathbf{R}_1|} - \frac{Z_C}{|\mathbf{r} + \mathbf{R}_2|} - \frac{Z_C}{|\mathbf{r} - \mathbf{R}_2|} - \frac{Z_H}{|\mathbf{r} - \mathbf{R}_1|} \quad (2)$$

is the one-electron Hamiltonian with a given magnetic quantum number m and $\xi = \cos\theta$ [35], and $Z_C = 6$ and $Z_H = 1$ denote the charges of the C nucleus and H nucleus, respectively. The electron-electron Coulomb interaction $J(\mathbf{r}, t)$ and exchange interaction $K(\mathbf{r}, t)$ have the following formulas:

$$J(\mathbf{r}_1, t)\Psi_i(\mathbf{r}_1, t) = \sum_j^n \int \frac{|\Psi_j(\mathbf{r}_2, t)|^2}{\mathbf{r}_{12}} d\mathbf{r}_2 \Psi_i(\mathbf{r}_1, t), \quad (3)$$

$$K(\mathbf{r}_1, t)\Psi_i(\mathbf{r}_1, t) = \sum_j^n \int \frac{\Psi_j^*(\mathbf{r}_2, t)\Psi_i(\mathbf{r}_2, t)}{\mathbf{r}_{12}} d\mathbf{r}_2 \Psi_j(\mathbf{r}_1, t), \quad (4)$$

where n indicates the total number of molecular occupied orbitals.

In our calculations, the i molecular orbital wave function $\Psi_i(\mathbf{r}, t)$ can be expanded in terms of the finite-element discrete-variable representation (FEDVR) basis and B-splines as [35]

$$\Psi_i(r, \xi, \varphi, t) = \frac{1}{\sqrt{2\pi}} \sum_{\mu\nu} C_{\mu\nu}^i(t) \frac{\chi_\mu(r)}{r} B_\nu^k(\xi) (1-\xi^2)^{|m|/2} e^{im\varphi}. \quad (5)$$

The details of FEDVR $\chi_\mu(r)$ and B-splines $B_\nu^k(\xi)$ can be found in [35,51,52]. The time-dependent wave function is propagated using the Crank-Nicolson method [35,52,53] and the orthogonality between different orbitals is enforced during the time evolution. A detailed introduction of the TDHF theory can be found in our previous works [34–36]. A $\cos^{1/8}$ mask function is used near the boundary to avoid unphysical reflection of the electronic wave packet.

After obtaining the time-varying wave functions $\Psi_i(\mathbf{r}, t)$, the time-dependent ionization probability of the i orbital is defined as

$$P_i(t) = 1 - \eta_i(t), \quad (6)$$

where $\eta_i(t) = \langle \Psi_i(\mathbf{r}, t) | \Psi_i(\mathbf{r}, t) \rangle$ is the time-varying population (survival probability) of orbital i in the simulation “box.” Then the total ionization probability is given by $P_{\text{total}}(t) = 1 - \prod_i \eta_i(t)$. The time-dependent orbital energy $\varepsilon_i(t)$ can be given by

$$\varepsilon_i(t) = \langle \Psi_i(\mathbf{r}, t) | H_0(\mathbf{r}) + 2J(\mathbf{r}, t) - K(\mathbf{r}, t) | \Psi_i(\mathbf{r}, t) \rangle. \quad (7)$$

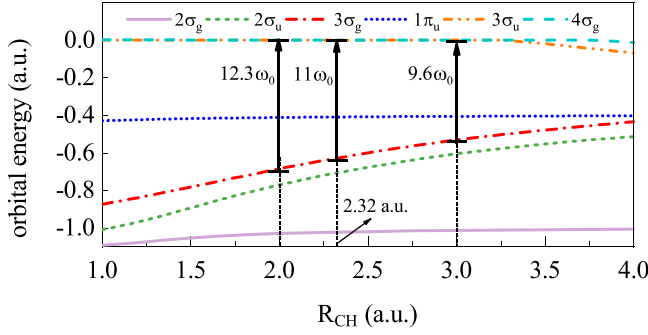


FIG. 2. The field-free orbital energies $\varepsilon_i(t=0)$ as a function of R_{CH} with the fixed $R_{CC} = 2.27$ a.u. The three vertical black arrows indicate the energy required for the electron to be excited from $3\sigma_g$ to $3\sigma_u$ when R_{CH} is 2.0 (equilibrium bond length), 2.32, and 3.0 a.u., respectively.

We also calculate the component of the n th field-free orbital $\Psi_n(\mathbf{r}, t=0)$ contained by the i time-dependent orbital $\Psi_i(\mathbf{r}, t)$, called the projected population, as follows:

$$P_{ni}(t) = |\langle \Psi_n(\mathbf{r}, t=0) | \Psi_i(\mathbf{r}, t) \rangle|^2. \quad (8)$$

The high harmonic spectra can be obtained by Fourier transforming the time-dependent dipole acceleration [17],

$$S(\omega) \propto \left| \int_0^T \sum_i a_i(t) e^{-i\omega t} dt \right|^2, \quad (9)$$

where $a_i(t) = \frac{d^2}{dt^2} \langle \Psi_i(\mathbf{r}, t) | Z | \Psi_i(\mathbf{r}, t) \rangle$ is the i orbital dipole acceleration.

In the following calculations, 134 FEDVR bases and 30 B-splines of the order of $k=7$ are used, the time step is 0.1 a.u., and the truncated radius is $r_{\max} = 50$ a.u. Convergence of numerical simulations is reached with the above settings.

III. RESULTS AND DISCUSSIONS

The electronic configuration of the ground state of C_2H_2 is $(1\sigma_g)^2(1\sigma_u)^2(2\sigma_g)^2(2\sigma_u)^2(3\sigma_g)^2(1\pi_u)^4$ and the LUMOs are $(3\sigma_u)^0$ and $(4\sigma_g)^0$. In Sec. III A, we investigate the HHG of C_2H_2 molecules in the monochromatic laser field for two groups of bond lengths: One is that the R_{CH} changes with the R_{CC} fixed at the equilibrium bond length, and another one is that both R_{CC} and R_{CH} are varied simultaneously. In Sec. III B, we investigate the influence of the 2ω field on the efficiency of HHG by introducing two-color fields.

A. The monochromatic laser field

The monochromatic laser field is selected to be linearly polarized along the molecular axis Z and the electric field is given by

$$E_{\text{mono}}(t) = E_0 f(t) \cos(\omega_0 t), \quad (10)$$

where E_0 indicates the peak field amplitude, ω_0 is the carrier frequency, and the envelope $f(t)$ is a six-optical-cycle trapezoidal pulse with one cycle ramp on, four cycles constant, and one cycle ramp off.

In Fig. 2, we plot the R_{CH} -dependent field-free energies $\varepsilon_i(t=0)$ of selected orbitals ($2\sigma_g$, $2\sigma_u$, $3\sigma_g$, $1\pi_u$, $3\sigma_u$, and

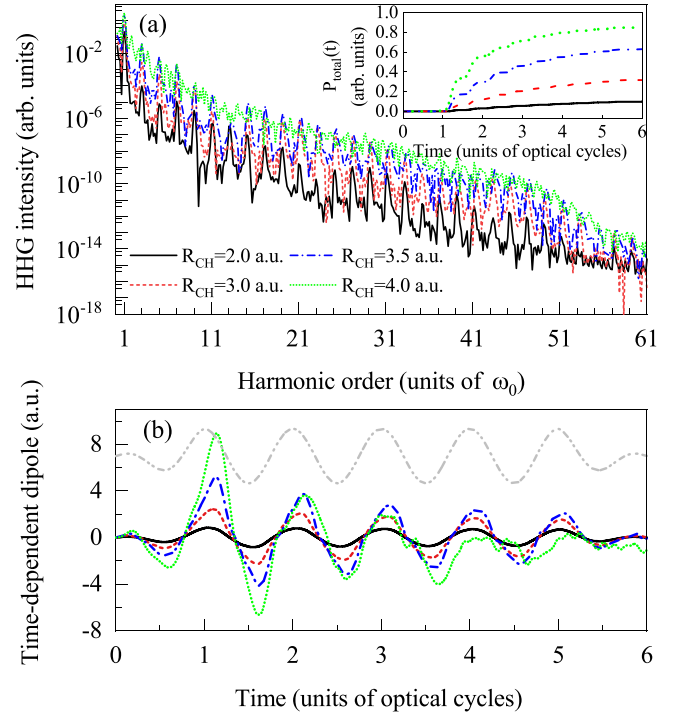


FIG. 3. (a) The total harmonic spectra of C_2H_2 molecules with different R_{CH} and fixed $R_{CC} = 2.27$ a.u. for the six-optical-cycle laser pulse with a peak intensity of 172 TW/cm^2 and a wavelength of 800 nm. For clarity, we only show the harmonic spectra of $R_{CH} = 2.0, 3.0, 3.5,$ and 4.0 a.u. The inset is the total time-dependent ionization probability $P_{\text{total}}(t)$. (b) The total time-dependent dipole of C_2H_2 with the same R_{CC} and R_{CH} as (a). The laser field is represented by the gray double-dot-dashed lines of (b).

$4\sigma_g$) with the fixed $R_{CC} = 2.27$ a.u. It is shown that as the C-H bond length is stretched, the orbital energies of $2\sigma_u$ and $3\sigma_g$ increase, while the orbital energies of $2\sigma_g$ and $1\pi_u$ change little. The energy gaps between $3\sigma_g$ ($2\sigma_u$) and $3\sigma_u$ ($4\sigma_g$) decrease with the increase of R_{CH} . The ionization energy of the $2\sigma_g$ electron is much larger with respect to those of electrons in the occupied orbitals $2\sigma_u$, $3\sigma_g$, and $1\pi_u$ in Fig. 2, so the $1\sigma_g$, $1\sigma_u$, and $2\sigma_g$ orbitals keep frozen in the time evolution of TDHF equations.

Figure 3(a) presents the total harmonic spectra of C_2H_2 molecules at the fixed $R_{CC} = 2.27$ a.u. and different R_{CH} ($R_{CH} = 2.0, 3.0, 3.5,$ and 4.0 a.u.) under the peak electric field of $E_0 = 0.07$ a.u. corresponding to the laser intensity of 172 TW/cm^2 for the wavelength of 800 nm. It can be seen that the harmonic intensity enhances with the increase of C-H bond lengths, which stems from the increased ionization probability [see the inset of Fig. 3(a)]. However, the enhancement of harmonic yield is not obvious when the C-H bond length is stretched from 3.5 to 4.0 a.u. In Fig. 3(b), we plot the total time-dependent dipoles at different C-H bonding lengths corresponding to Fig. 3(a). It can be seen that the dipoles adiabatically follow the external laser field at $R_{CH} = 2.0, 3.0,$ and 3.5 a.u., while the time-dependent dipole shows the subcycle oscillations in the last three cycles for $R_{CH} = 4.0$ a.u. Thus, the destruction of the periodic behavior of the electron results in the non-odd harmonics of the total

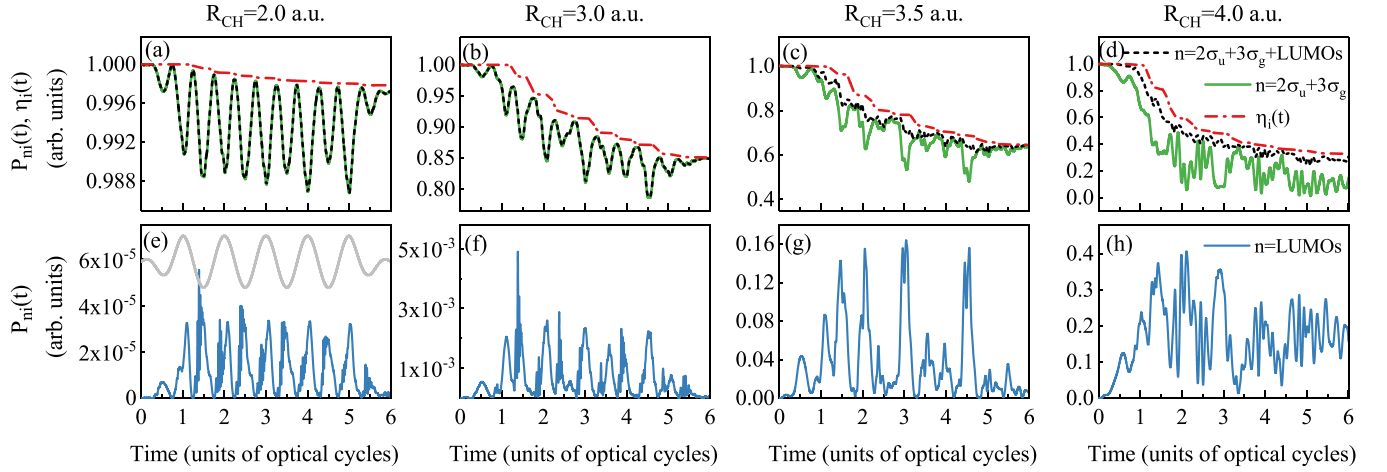


FIG. 4. The time-dependent population of $\eta_{3\sigma_g}(t)$ (red dot-dashed lines) of the $3\sigma_g$ orbital [$i = \Psi_{3\sigma_g}(\mathbf{r}, t)$] and the projections $P_{ni}(t)$ of the $\Psi_{3\sigma_g}(\mathbf{r}, t)$ on the two ground-state occupied orbitals ($n = 2\sigma_u + 3\sigma_g$, solid green lines), the two LUMOs ($n = \text{LUMOs}$, solid blue lines), and these four σ orbitals ($n = 2\sigma_u + 3\sigma_g + \text{LUMOs}$, dashed black lines) for different C-H bonding lengths. (a),(e) $R_{\text{CH}} = 2.0$ a.u.; (b),(f) $R_{\text{CH}} = 3.0$ a.u.; (c),(g) $R_{\text{CH}} = 3.5$ a.u.; (d),(h) $R_{\text{CH}} = 4.0$ a.u. The laser field is represented by the solid gray lines of (e) and the laser parameters are the same as those in Fig. 3. Here the R_{CC} is fixed at 2.27 a.u. In (a) and (b), the solid green lines nearly coincide with the dashed black lines.

spectrum when R_{CH} is 4.0 a.u. [see Fig. 3(a)]. Furthermore, close inspection of Fig. 3(b) reveals that the first amplitude of the dipole increases with the C-H bond length, which stems from the higher ionization rate near the $1T$ (T is the optical cycle) at large C-H bond lengths [see the inset of Fig. 3(a)]. We shall show below that ionization is closely related to the excitation from the inner σ orbitals to the LUMOs.

Since the ionization contribution of $1\pi_u$ can be ignored [47,49], we only consider the $2\sigma_u$, $3\sigma_g$, and LUMOs ($3\sigma_u$ and $4\sigma_g$). In Fig. 4, we present the time-dependent population $\eta_{3\sigma_g}(t)$ of the $\Psi_{3\sigma_g}(\mathbf{r}, t)$ orbital, the projected wave function $\Psi_{n,3\sigma_g}(t)$ of the time-dependent wave function $\Psi_{3\sigma_g}(\mathbf{r}, t)$ on the two occupied orbitals ($n = 2\sigma_u + 3\sigma_g$) (solid green lines), the two LUMOs ($n = \text{LUMOs}$) (solid blue lines), and four σ orbitals ($n = 2\sigma_u + 3\sigma_g + \text{LUMOs}$) (dashed black lines) for different R_{CH} with R_{CC} fixed at 2.27 a.u. The projections of the $\Psi_{2\sigma_u}(\mathbf{r}, t)$ on two occupied orbitals ($n = 2\sigma_u + 3\sigma_g$), the two LUMOs ($n = \text{LUMOs}$), and four σ orbitals ($n = 2\sigma_u + 3\sigma_g + \text{LUMOs}$) are similar to those of the $P_{n,3\sigma_g}(t)$, which are not shown here. For $R_{\text{CH}} = 2.0$ and 3.0 a.u., the components of the $2\sigma_u$ and $3\sigma_g$ states in the $\Psi_{3\sigma_g}(\mathbf{r}, t)$ orbital are dominant, while the population of the LUMOs is little. As R_{CH} reaches to 3.0 and 4.0 a.u., the populations of the two LUMOs increase significantly due to the decreasing of the energy gap between the $3\sigma_g$ and LUMOs (see Fig. 2). Additionally, the populations exhibit a strong oscillation at R_{CH} of 4.0 a.u., which is caused by the strong coupling between the $3\sigma_g$ orbital and LUMOs. Comparing Figs. 4(a)–4(d) with Figs. 4(e)–4(h), we can obtain the result that the decreased population of occupied orbitals ($2\sigma_u$ and $3\sigma_g$) corresponds to the increased population of the two LUMOs, so the electrons can be detached more easily through the channels of LUMOs. As a consequence, the ionization probability of $3\sigma_g$ electrons increases with the stretching C-H bond lengths due to the decreasing orbital ionization energy and the enhancement of the coupling between the $3\sigma_g$ orbital and the LUMOs.

Now let us turn to the distinct feature that the enhancement of harmonic yield is not obvious when the C-H bond length is stretched from 3.5 to 4.0 a.u. in Fig. 3(a). In order to observe the change of harmonic intensity with R_{CH} more intuitively, we calculate a smoothed harmonic spectrum where the peak structure has been eliminated [18], $S_{\text{smooth}}(\omega) = \int S(\tilde{\omega}) \exp[-(\tilde{\omega} - \omega)^2/\sigma^2] d\tilde{\omega}$, with $\sigma = 20\omega_0$. Then we integrate the intensity of plateau harmonics (from the 15th order to the 51st order) in the smoothed spectrum under different R_{CH} . In Fig. 5(a), the integral total $S_{\text{smooth}}(\omega)$ and the contribution from the $2\sigma_u$ and $3\sigma_g$ orbitals with respect to the R_{CH} are presented. It can be seen that the total harmonic intensity is dominated by the $2\sigma_u$ and $3\sigma_g$ orbitals. Moreover, the increase in the total harmonic intensity is insignificant when R_{CH} changes from 3.5 to 4.0 a.u. In Fig. 5(b), we show the ionization probability $P_i(t_{\text{end}})$ of different molecular orbitals and the total ionization probability $P_{\text{total}}(t_{\text{end}})$ with respect to R_{CH} at the end of the laser pulse. It is found that the ionization probability of the $2\sigma_u$ and $3\sigma_g$ electrons gradually exceeds that of the $1\pi_u$ electrons with increasing R_{CH} . The total ionization probability also increases with the C-H bond length stretched and is close to 1.0 when the R_{CH} is 4.0 a.u. In the spirit of the three-step model, the harmonic intensity is determined by the ionization, propagating, and recombination processes. Too high ionization probability of the electrons can lead to the strong depletion of the ground-state population, which will suppress the recombination process. In Fig. 5(c), we plot the sum of the projections of the final state wave function $\Psi_{3\sigma_g}(\mathbf{r}, t_{\text{end}})$ [$\Psi_{2\sigma_u}(\mathbf{r}, t_{\text{end}})$] on the $2\sigma_u$ and $3\sigma_g$ states and two LUMOs for different R_{CH} . It can be seen that the populations of $\Psi_{3\sigma_g}(\mathbf{r}, t_{\text{end}})$ and $\Psi_{2\sigma_u}(\mathbf{r}, t_{\text{end}})$ become very small for $R_{\text{CH}} = 4.0$ a.u., which suppresses the increase of the total harmonic intensity in Fig. 5(a). Thus, the enhancement of harmonic intensity through the stretched C-H bond length is a delicate balance between the ionization probability and depletion of ground states.

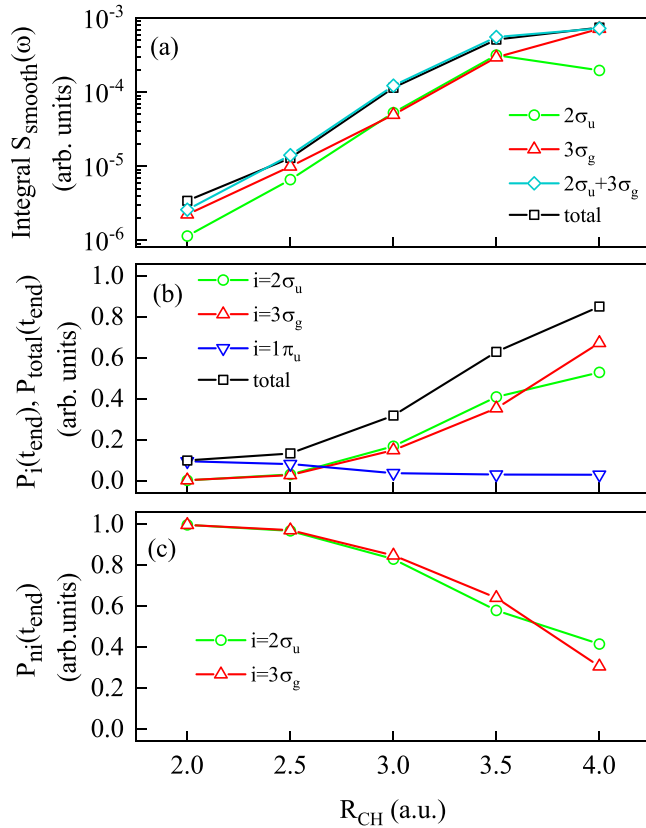


FIG. 5. (a) The integral total plateau intensity and the contribution from the $2\sigma_u$ and $3\sigma_g$ orbitals of the smoothed spectrum $S_{\text{smooth}}(\omega)$ for different R_{CH} (see text for the details). (b) Probabilities of the electron ionized from the i orbital $P_i(t_{\text{end}})$ and the total ionization probability $P_{\text{total}}(t_{\text{end}})$ after the conclusion of the laser pulse for different R_{CH} . (c) The sum of the projections of the final state wave function [$i = \Psi_{3\sigma_g}(\mathbf{r}, t_{\text{end}})$ or $\Psi_{2\sigma_u}(\mathbf{r}, t_{\text{end}})$] on the ground state $2\sigma_u$, $3\sigma_g$ and the two LUMOs ($n = 2\sigma_u + 3\sigma_g + \text{LUMOs}$) for different R_{CH} . The laser parameters are the same as those in Fig. 3. Here the R_{CC} is fixed at 2.27 a.u.

Because the photon energy of the 800 nm laser pulse is close to the energy gap between the $2\sigma_u$ and $3\sigma_g$ orbitals, the near single-photon resonance between the two orbitals can occur. In Fig. 6(a), we depict the projection $P_{n,3\sigma_g}(t)$ of the time-dependent wave function $\Psi_{3\sigma_g}(\mathbf{r}, t)$ on the field-free $2\sigma_u$ and $3\sigma_g$ orbitals for $R_{\text{CH}} = 2.0$ a.u., respectively. It is demonstrated that the populations of $3\sigma_g$ and $2\sigma_u$ orbitals exhibit a periodic Rabi oscillation. Furthermore, the instantaneous dipoles of the $2\sigma_u$ and $3\sigma_g$ orbitals in Fig. 6(b) exhibit a strong nonadiabatic behavior, where the electrons localize at one side of the molecule for longer than a half optical cycle. The transient electron localization breaks the symmetry of the $2\sigma_u$ and $3\sigma_g$ orbitals. As a result, the non-odd harmonics show up in the harmonic spectra of $2\sigma_u$ and $3\sigma_g$ in Fig. 6(c). Similar phenomena have been observed in the harmonic spectra of H_2^+ [54] and open-shell molecules [55] owing to the resonant coupling of different orbitals. However, the sum dipole [see Fig. 6(b)] of the $2\sigma_u$ and $3\sigma_g$ orbitals is an adiabatic response to the field because of the destructive interference between the time-varying dipoles of the two orbitals, which gives rise

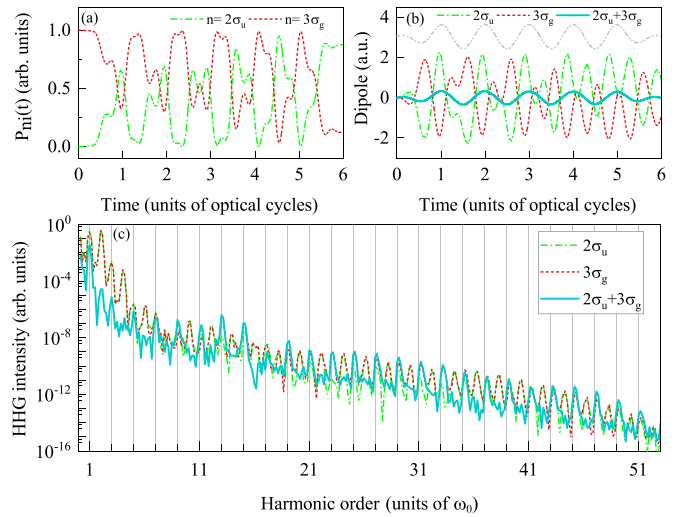


FIG. 6. (a) Projected population $P_{ni}(t)$ of the time-dependent $3\sigma_g$ wave function [$i = \Psi_{3\sigma_g}(\mathbf{r}, t)$] on the field-free orbitals ($n = 2\sigma_u$ or $3\sigma_g$) of C_2H_2 with $R_{\text{CH}} = 2.0$ a.u. (b) The time-dependent dipoles. (c) The harmonic components of $2\sigma_u$ and $3\sigma_g$ for C_2H_2 with $R_{\text{CH}} = 2.0$ a.u. and the coherent sum of these two orbitals. The laser field is represented by the gray double-dot-dashed lines of (b) and the laser parameters are the same as those in Fig. 3. The vertical gray lines of (c) indicate the odd harmonics. Here the R_{CC} is fixed at 2.27 a.u.

to the disappearance of the non-odd harmonics in the sum harmonic spectrum [see Fig. 6(c)].

Next we carry out the calculations that the C-C and C-H bond lengths are stretched simultaneously. In our calculations, the internuclear separations of $(R_{\text{CH}}, R_{\text{CC}}) = (2.0, 2.27)$, $(2.5, 2.77)$, $(3.0, 3.27)$, $(3.25, 3.52)$, and $(3.5, 3.77)$ a.u. are considered. Figure 7 shows the field-free orbital energies with the internuclear distances of R_{CH} and R_{CC} stretched simultaneously. Comparing Fig. 7 with Fig. 2, we can see that the orbital energy of $2\sigma_u$ changes slowly with simultaneously increasing R_{CH} and R_{CC} , and the energy difference between $3\sigma_g$ and $3\sigma_u$ is smaller than that of Fig. 2 at the larger R_{CH} . Also, we perform the same calculations as in Fig. 5. As shown in Fig. 8(a), the total harmonic intensity is dominated by the

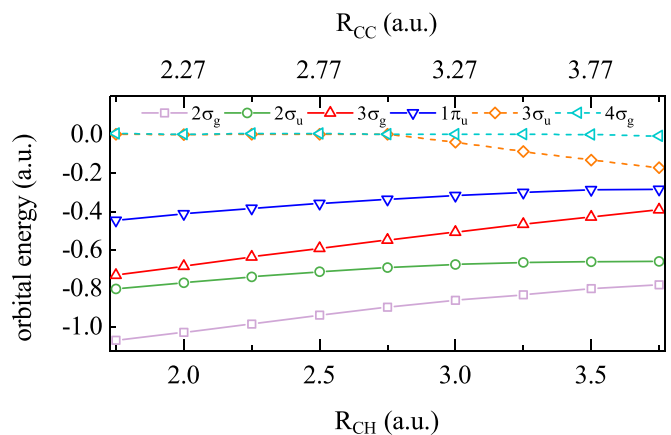


FIG. 7. The field-free orbital energies $\epsilon_i(t=0)$ as a function of internuclear distances $(R_{\text{CH}}, R_{\text{CC}})$ (see text for more details).

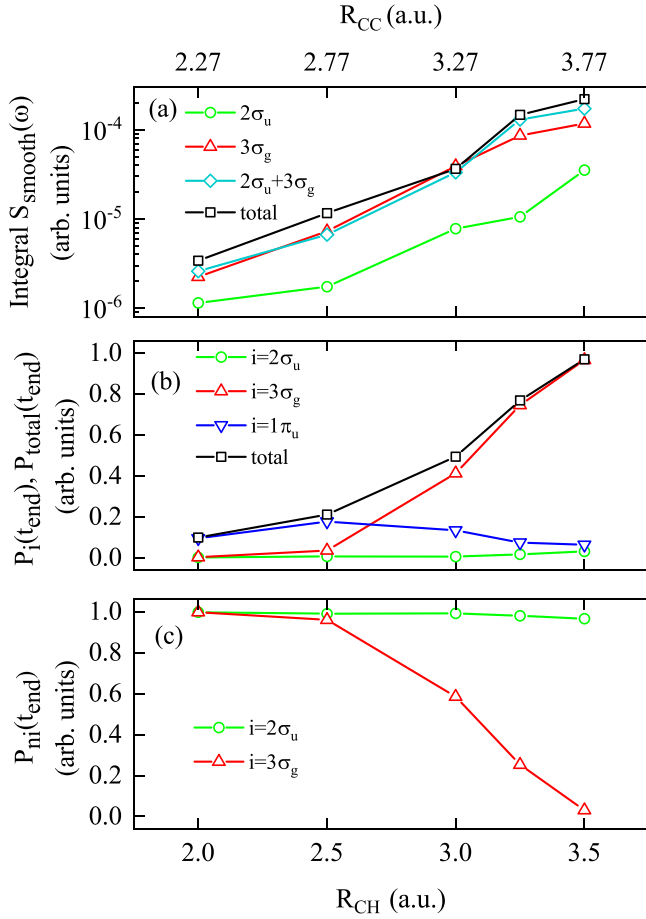


FIG. 8. Same as Fig. 5, except for changing R_{CC} and R_{CH} simultaneously in the calculations (see text for more details).

contribution of the $3\sigma_g$ orbital with respect to the contribution of the $2\sigma_u$ orbital. The reason is that the orbital energy of $2\sigma_u$ in Fig. 7 increases more slowly with the bonding lengths stretched compared with that shown in Fig. 2, resulting in a lower ionization probability than that of the $3\sigma_g$ electrons [see Fig. 8(b)]. Moreover, the total harmonic intensity also reaches a plateau with the increase of R_{CC} and R_{CH} due to the depletion of the ground-state population [see Fig. 8(c)]. Comparing Fig. 5(c) with Fig. 8(c), we see that the depletion of the time-dependent $3\sigma_g$ with simultaneously increasing R_{CH} and R_{CC} is stronger than the case of only the C-H bond length stretched while the C-C bond length remains fixed at the equilibrium distance. This is because the former has a smaller energy gap between $3\sigma_g$ and $3\sigma_u$ orbitals at larger bonding length, as shown in Fig. 7.

In short, the intensity of the total harmonic spectrum is enhanced with the increase of the C-H bond lengths, which stems from the high ionization probability of the $2\sigma_u$ and $3\sigma_g$ electrons due to their decreasing ionization energies and the strong coupling through the channels of LUMOs. Moreover, the enhancement in harmonic efficiency is limited by the depletion of the ground-state population.

B. Two-color laser fields

Considering the importance of excitation on ionization as shown in Fig. 4, we attempt to increase the harmonic in-

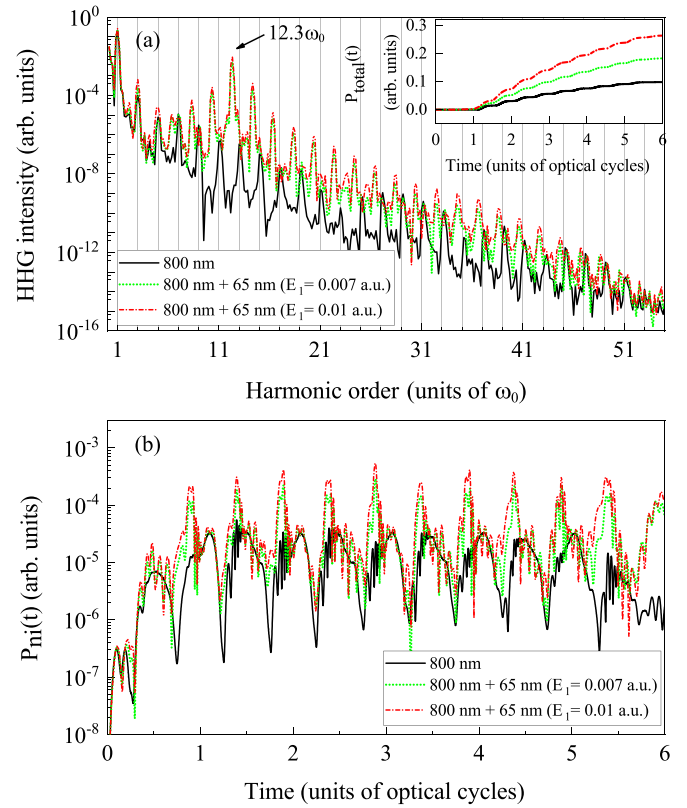


FIG. 9. (a) The total harmonic spectra of the C_2H_2 molecule with $R_{CH} = 2.0$ a.u. and $R_{CC} = 2.27$ a.u. subjected to two-color fields as shown in Eq. (11): ω_1 is 0.7 a.u. corresponding to a wavelength of 65 nm and E_1 is 0.007 and 0.01 a.u., respectively. For comparison, we also show the total harmonic spectrum of the C_2H_2 molecule with $R_{CH} = 2.0$ in the monochromatic 800 nm laser field. The vertical gray lines indicate the odd harmonics. The inset is the total time-dependent ionization probability $P_{total}(t)$. (b) Projected population $P_{ni}(t)$ of the time-dependent $3\sigma_g$ wave function [$i = \Psi_{3\sigma_g}(\mathbf{r}, t)$] on two LUMOs ($n = \text{LUMOs}$) in logarithmic scales.

tensity of the C_2H_2 molecules with $R_{CH} = 2.0$ and 3.0 a.u. with the fixed $R_{CC} = 2.27$ a.u. by introducing a two-color field scheme, in which the frequency of the second field corresponds to the energy gap between the $3\sigma_g$ and $3\sigma_u$ orbitals. Such a scheme has been applied in the atomic harmonic spectra, in which the harmonic efficiency can be enhanced by several orders of magnitude with an auxiliary XUV field [56–62].

The two-color laser field is assumed to be written as

$$E_{two}(t) = E_{mono}(t) + E_1 f(t) \cos(\omega_1 t), \quad (11)$$

where E_1 and ω_1 indicate the peak field amplitude and frequency of the XUV pulse, respectively. The polarization direction of the XUV field is parallel to the monochromatic field $E_{mono}(t)$. The parameters of $E_{mono}(t)$ are fixed at 800 nm wavelength and $E_0 = 0.07$ a.u. For the XUV field, the ω_1 is set to match the energy gap between $3\sigma_g$ and $3\sigma_u$, i.e., $\omega_1 = 0.7$ a.u. (corresponding to 65 nm wavelength) at $R_{CH} = 2.0$ a.u. and $\omega_1 = 0.55$ a.u. (corresponding to 83 nm wavelength) at $R_{CH} = 3.0$ a.u., respectively.

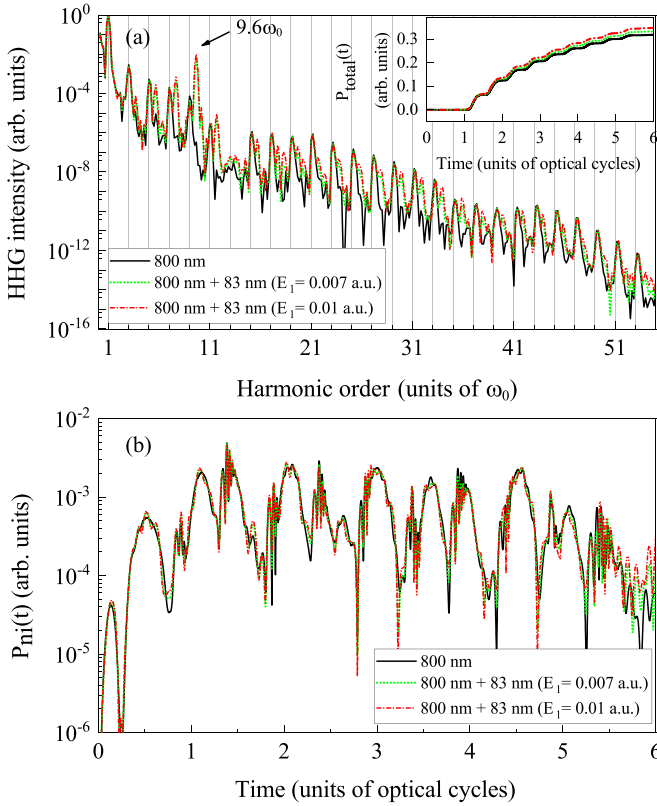


FIG. 10. Same as Fig. 9, except for the C_2H_2 molecule with $R_{\text{CH}} = 3.0$ a.u. subjected to two-color fields as shown in Eq. (11): ω_1 is 0.55 a.u., corresponding to a wavelength of 83 nm, and E_1 is 0.007 and 0.01 a.u., respectively.

Figure 9(a) shows the total harmonic spectra of C_2H_2 with $R_{\text{CH}} = 2.0$ a.u. and $R_{\text{CC}} = 2.27$ a.u. under two-color fields with $E_1 = 0.007$ and 0.01 a.u. corresponding to laser intensities of 1.72 TW/cm 2 and 3.5 TW/cm 2 , respectively. It can be seen that an obvious peak appears in the harmonic spectra and the frequency (about $12.3\omega_0$, indicated by the arrow) of the peak harmonic corresponds to the energy difference between the $3\sigma_g$ and $3\sigma_u$ orbitals. Thus, the peak is attributed to the resonance effect between the $3\sigma_g$ and $3\sigma_u$ orbitals induced by the 65 nm XUV field and the distribution of the remaining harmonics is symmetric around the peak [60,62]. Moreover, the whole harmonic spectra yields are enhanced with the increase of XUV field intensity. To uncover this enhancement mechanism, we plot the sum of the projected population of $\Psi_{3\sigma_g}(\mathbf{r}, t)$ on the two LUMOs in logarithmic scales in Fig. 9(b). The projection of the $\Psi_{2\sigma_u}(\mathbf{r}, t)$ is similar to the $P_{n,3\sigma_g}(t)$, so it is not shown here. From Fig. 9(b), we can see that the populations of the two LUMOs increase with the enhancement of the XUV field intensity. Therefore, the increase of the populations of the two LUMOs induced by the XUV field leads to the higher ionization [see the inset of Fig. 9(a)], which gives rise to the enhancement of the HHG emission.

Furthermore, we also show the case of $R_{\text{CH}} = 3.0$ a.u. in Fig. 10. By comparing the spectrum of the monochromatic field with the spectra of the two-color laser fields with different XUV laser intensities, it can be seen that the variation of

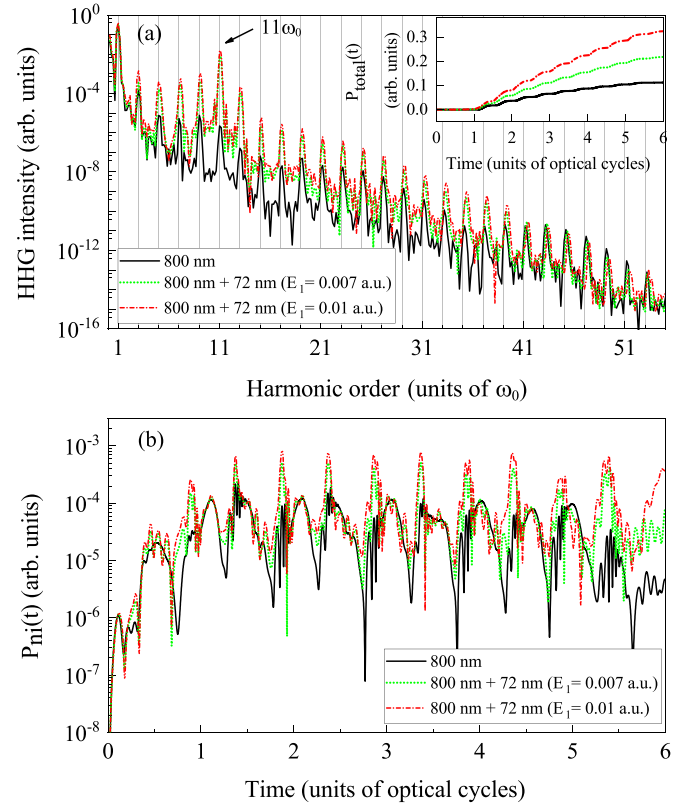


FIG. 11. Same as Fig. 9, except for the C_2H_2 molecules with $R_{\text{CH}} = 2.32$ a.u. subjected to two-color fields as shown in Eq. (11): ω_1 is 0.63 a.u., corresponding to a wavelength of 72 nm, and E_1 is 0.007 and 0.01 a.u., respectively.

the harmonic spectrum is not obvious except for the resonance peak (about $9.6\omega_0$, indicated by the arrow) and some weak peaks symmetrically distributed around the peak. The inset of Fig. 10(a) shows the comparison of the ionization probability of the monochromatic field with that of the two-color fields, which indicates that the change of the ionization probability is little considering the two-color field. Furthermore, we plot the projections of $\Psi_{3\sigma_g}(\mathbf{r}, t)$ on the two LUMOs in two-color fields and a monochromatic field in Fig. 10(b), which also shows that the changes of populations are not obvious at different laser pulses. For $R_{\text{CH}} = 3.0$ a.u., the electrons of the $\Psi_{3\sigma_g}(\mathbf{r}, t)$ orbital are more probable to be excited into the two LUMOs in the monochromatic field due to the smaller energy gap between the $3\sigma_g$ orbital and the LUMOs with respect to the case of $R_{\text{CH}} = 2.0$ a.u. As a result, in order to cause an obvious increase of the efficiency of harmonic emission, a more intense XUV laser intensity is necessary in the case of $R_{\text{CH}} = 3.0$ a.u.

In addition, it is worthwhile to mention that the frequencies of the selected 65 or 83 nm XUV field and the 800 nm infrared field are incommensurate, and the apparent effect of the incoherence of the two light sources is seen in Figs. 9(a) and 10(a) where the harmonic peaks are no longer purely aligned with the odd multiple frequency of 800 nm under the two-color field, so these harmonic peaks do not represent the real harmonics of the infrared laser field. Moreover, such a two-color field does not repeat each infrared field cycle, so the

shape of the two-color laser pulse will depend on the actual laser parameters in the experiment, such as the pulse duration. For this reason, we have carried out additional calculations for the XUV field with the odd multiple frequency of 800 nm. We set the frequency of the XUV field to $11\omega_0$ (corresponding to 72 nm wavelength), which matches the energy gap of 0.63 a.u. between the $3\sigma_g$ and $3\sigma_u$ orbitals at $R_{CH} = 2.32$ a.u., as shown in Fig. 2. The harmonic spectra are shown in Fig. 11. It can be seen that the odd harmonic peaks are very obvious in the whole harmonic spectrum for the two-color field, and the enhancement of harmonic intensity in Fig. 11(a) stems from the large ionization probabilities of C_2H_2 molecules exposed to two-color fields [see the inset of Fig. 11(a)], which is ascribed to the strong coupling between the $3\sigma_g$ and LUMOs induced by the XUV fields in Fig. 11(b).

In Ref. [50], the authors have shown that the excitation from $3\sigma_g$ to $3\sigma_u$ plays a crucial role in the HHG of C_2H_2 and the inner plateau intensity is increased by adding a vacuum ultraviolet pump pulse before the midinfrared pulse that generates harmonics. Here, we provide another approach to enhance the efficiency of harmonic emission based on our results of two-color fields. It is worthwhile to mention that the C_2H_2 molecule with large C-H bond length can be achieved experimentally by the following scheme. A laser pulse is first adopted to pump the C_2H_2 molecule to an excited state, and then it begins to dissociate. When the C-H bond length is stretched far enough, another laser pulse is applied to bring the C_2H_2 molecule back to the ground state.

IV. CONCLUSIONS

In summary, we have systematically investigated the high harmonic generation of stretched C_2H_2 molecules by numerically solving the TDHF equations. It is found that as the C-H bond lengths are stretched, the harmonic intensity enhances significantly, which stems from the increased ionization probability of the HOMO-1 ($3\sigma_g$) and HOMO-2

($2\sigma_u$) orbitals due to their decreasing ionization energies and the excitation channels of the LUMOs in the monochromatic field. However, the enhancement in harmonic intensity will be limited by the strong depletion of the ground-state population at the large C-H bonding length, and the above phenomenon also occurs when the C-H and C-C bonding lengths are stretched simultaneously. In addition, the nonadiabatic effect induced by the laser coupling among several orbitals leads to the non-odd harmonics. In the scheme of two-color laser fields, we investigate the modulation of the harmonic intensity caused by the XUV field for C_2H_2 for different C-H bonding lengths with the C-C bonding length fixed at the equilibrium distance. It is found that the excitation of $3\sigma_g$ electrons into the LUMOs induced by the XUV field can lead to the enhancement of the harmonic efficiency. Because the energy gap between the $3\sigma_g$ and the two LUMOs of $R_{CH} = 3.0$ a.u. is smaller than the case of $R_{CH} = 2.0$ a.u., a stronger XUV field is necessary for the former in order to cause a more dramatic increase of harmonic intensity than the monochromatic field. Our work indicates the important role of excitation from occupied orbital to LUMOs in molecular harmonic spectra, and introduces another approach to enhance the efficiency of harmonic emission for polyatomic molecules exposed to intense laser pulses.

ACKNOWLEDGMENTS

This work was supported by the National Key Research and Development program (Grant No. 2019YFA0307700), the National Natural Science Foundation of China (Grant No. 11804405), Project of Thousand Youth Talents in China, HPC Platform of ShanghaiTech University, the Key-Area Research and Development Program of Guangdong Province under Grant No. 2019B030330001, and the Science and Technology Program of Guangzhou (China) under Grant No. 201904020024.

-
- [1] F. Krausz and M. Ivanov, *Rev. Mod. Phys.* **81**, 163 (2009).
 - [2] J. Itatani, J. Levesque, D. Zeidler, H. Niikura, H. Pépin, J. C. Kieffer, P. B. Corkum, and D. M. Villeneuve, *Nature (London)* **432**, 867 (2004).
 - [3] S. Baker, J. S. Robinson, C. A. Haworth, H. Teng, R. A. Smith, C. C. Chirila, M. Lein, J. W. G. Tisch, and J. P. Marangos, *Science* **312**, 424 (2006).
 - [4] M. Lein, *J. Phys. B: At. Mol. Opt. Phys.* **40**, R135 (2007).
 - [5] C. Vozzi, M. Negro, F. Calegari, G. Sansone, M. Nisoli, S. D. Silvestri, and S. Stagira, *Nat. Phys.* **7**, 822 (2011).
 - [6] O. Smirova, Y. Mairesse, S. Patchkovskii, N. Dudovich, D. Villeneuve, P. Corkum, and M. Y. Ivanov, *Nature (London)* **460**, 972 (2009).
 - [7] P. B. Corkum, *Phys. Rev. Lett.* **71**, 1994 (1993).
 - [8] H. Akagi, T. Otobe, A. Staudte, A. Shiner, F. Turner, R. Dörner, D. M. Villeneuve, and P. B. Corkum, *Science* **325**, 1364 (2009).
 - [9] L. Torlina, M. Ivanov, Z. B. Walters, and O. Smirnova, *Phys. Rev. A* **86**, 043409 (2012).
 - [10] H. J. Wörner, J. B. Bertrand, P. Hockett, P. B. Corkum, and D. M. Villeneuve, *Phys. Rev. Lett.* **104**, 233904 (2010).
 - [11] Y. Mairesse, J. Higué, N. Dudovich, D. Shafir, B. Fabre, E. Mével, E. Constant, S. Patchkovskii, Z. Walters, M. Y. Ivanov, and O. Smirnova, *Phys. Rev. Lett.* **104**, 213601 (2010).
 - [12] B. D. Bruner, Z. Mašín, M. Negro, F. Morales, D. Brambila, M. Devetta, D. Faccialà, A. G. Harvey, M. Ivanov, Y. Mairesse, S. Patchkovskii, V. Sebinenko, H. Soifer, S. Stagira, C. Vozzi, N. Dudovich, and O. Smirnova, *Faraday Discuss.* **194**, 369 (2016).
 - [13] M. Ruberti, P. Decleva, and V. Averbukh, *Phys. Chem. Chem. Phys.* **20**, 8311 (2018).
 - [14] T. Zuo and A. D. Bandrauk, *Phys. Rev. A* **52**, R2511(R) (1995).
 - [15] A. Saenz, *Phys. Rev. A* **61**, 051402(R) (2000).
 - [16] E. Constant, H. Stapelfeldt, and P. B. Corkum, *Phys. Rev. Lett.* **76**, 4140 (1996).
 - [17] M. Lein, N. Hay, R. Velotta, J. P. Marangos, and P. L. Knight, *Phys. Rev. Lett.* **88**, 183903 (2002).

- [18] M. Lein, N. Hay, R. Velotta, J. P. Marangos, and P. L. Knight, *Phys. Rev. A* **66**, 023805 (2002).
- [19] T. Kanai, S. Minemoto, and H. Sakai, *Nature (London)* **435**, 470 (2005).
- [20] M. Lein, *Phys. Rev. Lett.* **94**, 053004 (2005).
- [21] J. E. Reutt, L. S. Wang, J. E. Pollard, D. J. Trevor, Y. T. Lee, and D. A. Shirley, *J. Chem. Phys.* **84**, 3022 (1986).
- [22] S. Baker, J. S. Robinson, M. Lein, C. C. Chirilă, R. Torres, H. C. Bandulet, D. Comtois, J. C. Kieffer, D. M. Villeneuve, J. W. G. Tisch, and J. P. Marangos, *Phys. Rev. Lett.* **101**, 053901 (2008).
- [23] H. Ahmadi, A. Maghari, H. Sabzyan, A. R. Niknam, and M. Vafae, *Phys. Rev. A* **90**, 043411 (2014).
- [24] D. A. Telnov, J. Heslar, and S.-I. Chu, *Phys. Rev. A* **95**, 043425 (2017).
- [25] X.-Y. Miao and H.-N. Du, *Phys. Rev. A* **87**, 053403 (2013).
- [26] J. Guo, X.-L. Ge, H. Zhong, X. Zhao, M. Zhang, Y. Jiang, and X.-S. Liu, *Phys. Rev. A* **90**, 053410 (2014).
- [27] X.-B. Bian and A. D. Bandrauk, *Phys. Rev. Lett.* **113**, 193901 (2014).
- [28] L. He, Q. Zhang, P. Lan, W. Cao, X. Zhu, C. Zhai, F. Wang, W. Shi, M. Li, X.-B. Bian, P. Lu, and A. D. Bandrauk, *Nat. Commun.* **9**, 1108 (2018).
- [29] C. B. Madsen and L. B. Madsen, *Phys. Rev. A* **74**, 023403 (2006).
- [30] C. B. Madsen, M. Abu-samha, and L. B. Madsen, *Phys. Rev. A* **81**, 043413 (2010).
- [31] S. Patchkovskii, *Phys. Rev. Lett.* **102**, 253602 (2009).
- [32] S. Patchkovskii and M. S. Schuurman, *Phys. Rev. A* **96**, 053405 (2017).
- [33] K. C. Kulander, *Phys. Rev. A* **36**, 2726 (1987).
- [34] S. L. Hu, Z. X. Zhao, and T. Y. Shi, *Intl. J. Quantum Chem.* **114**, 441 (2014).
- [35] S. L. Hu, Z. X. Zhao, J. Chen, and T. Y. Shi, *Phys. Rev. A* **92**, 053409 (2015).
- [36] J. Li, Z. Shu, S. Hu, C. Bi, A. Huang, Z. Xiao, J. Chen, and X. Liu, *J. Phys. B: At. Mol. Opt. Phys.* **53**, 195601 (2020).
- [37] C. Vozzi, R. Torres, M. Negro, L. Brugnera, T. Siegel, C. Altucci, R. Velotta, F. Frassetto, L. Poletto, P. Villoresi, S. D. Silvestri, S. Stagira, and J. P. Marangos, *Appl. Phys. Lett.* **97**, 241103 (2010).
- [38] R. Torres, T. Siegel, L. Brugnera, I. Procino, J. G. Underwood, C. Altucci, R. Velotta, E. Springate, C. Froud, I. C. E. Turcu, M. Y. Ivanov, O. Smirnova, and J. P. Marangos, *Opt. Express* **18**, 3174 (2010).
- [39] I. Bocharova, R. Karimi, E. F. Penka, J.-P. Brichta, P. Lassonde, X. Fu, J.-C. Kieffer, A. D. Bandrauk, I. Litvinyuk, J. Sanderson, and F. Légaré, *Phys. Rev. Lett.* **107**, 063201 (2011).
- [40] S. Roither, X. Xie, D. Kartashov, L. Zhang, M. Schöffler, H. Xu, A. Iwasaki, T. Okino, K. Yamanouchi, A. Baltuska, and M. Kitzler, *Phys. Rev. Lett.* **106**, 163001 (2011).
- [41] S. Bubin, M. Atkinson, K. Varga, X. Xie, S. Roither, D. Kartashov, A. Baltuška, and M. Kitzler, *Phys. Rev. A* **86**, 043407 (2012).
- [42] X. Xie, S. Roither, M. Schöffler, H. Xu, S. Bubin, E. Lötstedt, S. Erattuphuza, A. Iwasaki, D. Kartashov, K. Varga, G. G. Paulus, A. Baltuška, K. Yamanouchi, and M. Kitzler, *Phys. Rev. A* **89**, 023429 (2014).
- [43] C. Cornaggia, *J. Phys. B: At. Mol. Opt. Phys.* **49**, 19LT01 (2016).
- [44] C. Burger, A. Atia-Tul-Noor, T. Schnappinger, H. Xu, P. Rosenberger, N. Haram, S. Beaulieu, F. Légaré, A. S. Alnaser, R. Moshhammer, R. T. Sang, B. Bergues, M. S. Schuurman, R. de Vivie-Riedle, I. V. Litvinyuk, and M. F. Kling, *Struct. Dyn.* **5**, 044302 (2018).
- [45] E. Lötstedt, T. Kato, and K. Yamanouchi, *Phys. Rev. A* **85**, 041402(R) (2012).
- [46] E. Lötstedt, T. Kato, and K. Yamanouchi, *Phys. Rev. A* **86**, 023401 (2012).
- [47] E. Lötstedt, T. Kato, and K. Yamanouchi, *J. Chem. Phys.* **138**, 104304 (2013).
- [48] A. Russakoff, S. Bubin, X. Xie, S. Erattupuzha, M. Kitzler, and K. Varga, *Phys. Rev. A* **91**, 023422 (2015).
- [49] S. Erattupuzha, C. L. Covington, A. Russakoff, E. Lötstedt, S. Larimian, V. Hanus, S. Bubin, M. Koch, S. Gräfe, A. Baltuška, X. Xie, K. Yamanouchi, K. Varga, and M. Kitzler, *J. Phys. B: At. Mol. Opt. Phys.* **50**, 125601 (2017).
- [50] P. Mulholland and D. Dundas, *Phys. Rev. A* **97**, 043428 (2018).
- [51] T. N. Rescigno and C. W. McCurdy, *Phys. Rev. A* **62**, 032706 (2000).
- [52] H. Bachau, E. Cormier, P. Decleva, J. E. Hansen, and F. Martín, *Rep. Prog. Phys.* **64**, 1815 (2001).
- [53] S. L. Hu, Z. Shu, M. Q. Liu, L. Guo, X. L. Hao, J. Chen, and C. H. Lee, *Opt. Express* **26**, 32225 (2018).
- [54] M. R. Miller, A. Jaroń-Becker, and A. Becker, *Mol. Phys.* **115**, 1758 (2017).
- [55] Y. Xia and A. Jaroń-Becker, *Opt. Express* **24**, 4689 (2016).
- [56] Z. Zeng, R. Li, Y. Cheng, W. Yu, and Z. Xu, *Phys. Scr.* **66**, 321 (2002).
- [57] K. Ishikawa, *Phys. Rev. Lett.* **91**, 043002 (2003).
- [58] K. Schiessl, E. Persson, A. Scrinzi, and J. Burgdörfer, *Phys. Rev. A* **74**, 053412 (2006).
- [59] E. J. Takahashi, T. Kanai, K. L. Ishikawa, Y. Nabekawa, and K. Midorikawa, *Phys. Rev. Lett.* **99**, 053904 (2007).
- [60] A. Fleischer, *Phys. Rev. A* **78**, 053413 (2008).
- [61] X.-S. Liu and N.-N. Li, *J. Phys. B: At. Mol. Opt. Phys.* **41**, 015602 (2008).
- [62] M. Tudorovskaya and M. Lein, *J. Mod. Opt.* **61**, 845 (2014).